Heliyon 9 (2023) e13274

Contents lists available at ScienceDirect

Heliyon

journal homepage: www.cell.com/heliyon

Research article

Dynamics of green spaces- Land surface temperature intensity nexus in cities of Ethiopia

Mekonnen Amberber Degefu [a,*], Mekuria Argaw [b], Gudina Legese Feyisa [b], Sileshi Degefa [b]

[a] Kotebe University of Education, Addis Ababa, Ethiopia
[b] Center for Environmental Science, Addis Ababa University, Addis Ababa, Ethiopia

ARTICLE INFO

Keywords:
Cities
Land surface temperature
Urban ecosystem
Spatial dependence

ABSTRACT

In this study, the dynamics of green spaces and land surface temperature patterns in four cities in Ethiopia were investigated using Landsat imagery. The typical characteristics of LST over the past three decades (1990–2020) in relation to green space dynamics were first investigated; subsequently, the spatial distribution of LST was characterized based on hybrid geospatial techniques and mono-window algorithm analysis, in which the contributions of green spaces to LST were studied. In addition, the multiple linear regression method and spatial regression models (SRMs) were employed to investigate and predict the spatial dependence of LST and urbanization-induced green space dynamics. Results show that cities horizontally expanded unceasingly from 1990 to 2020, with a substantial discrepancy in expansion rates and the spatial patterns of UHI intensities among the cities ($p < 0.05$). Moreover, the area proportion of the UHI is significantly larger than that of the UGS, and the differences in the UGS cooling contribution were found in different land uses and zones of the cities. In the study periods, the spatial pattern of LST was significantly controlled by NDBI, and its coefficient in the OLS followed the pattern NDVI > MNDWI > latitudes > longitudes > population density > DEM. Due to the large proportions of buildings While green land and water bodies show significant capability to mitigate UHI effects, cooling effects are not apparent when their sizes are small. Besides, the SRMs show that UHI intensities were significantly influenced by MNDWI in Bahir Dar and Hawassa ($p < 0.01$).Cities' LAMBDA coefficients have a positive relationship with UHII ($p < 0.01$). Our study could help city planners and the government understand the current cooling potential of existing UGS to mitigate the dynamics of UHI and sustain the sustainability of green space management in cities.

1. Introduction

Extreme heat is a growing threat to the health of urban ecosystems, particularly in densely populated and industrialized cities [1]. Urbanization can greatly influence the urban thermal environment by increasing land surface temperature [9,22,61], the composition, structure, and function of the urban ecosystem services [8], the energy flow between the land surface and the atmosphere [34], and overall urban ecosystem sustainability [8]. The most common phenomenon that increases the surface temperature of a city relative to its fringe is called the "urban heat island (UHI)" [34]; Oke, 1995). The main contributor to LST is anthropogenic heat sources, which

* Corresponding author.
E-mail address: gmekonnena@gmail.com (M.A. Degefu).

https://doi.org/10.1016/j.heliyon.2023.e13274
Received 20 July 2022; Received in revised form 23 January 2023; Accepted 24 January 2023
Available online 30 January 2023

include the heat emitted from industrial activity, human metabolism, and vehicle exhausts, as well as the reduction of offset potential in urban forests [20].

Conversely, urban green spaces (UGSs) are significant, nature-based solutions to climate change and have immense potential to reduce vulnerability to heat waves (the UHI effect) while enhancing the resilience of climate change [9]. However, the decline of green spaces is often induced by a human-related factor, such as accelerated urban expansion [58] which creates pressure on the existing resources and leads to the fragmentation of green spaces [8,58]. This tendency is more frequent in developing countries and especially prevalent in Africa. Thus, characterizing the dynamics of UHI and UGS associations is critical for mitigating the ongoing negative effects of the climate crisis [11,56].

Consquensly, UHI suffering the survival of all living organisms in the urban ecosystem [12,34]. For example, UHI influence the interspecific phenotypic plasticity and larval survival of butterflies [32], slow the development of widow spider [30], and disturbs the health of urban residents [44,69] and persuade nonfatal effects such as dehydration, heat strokes, and heat fatigue [46]. Thus, understanding characteristics of the spatial distribution of LST and influencing factors of LST pattern and evolution are important for sustainable urban policies development [11,61] and reduce the unabated negative influences of climate crisis [8,56,62]. Even though some studies have been conducted, the results focused on the linear relationship between LST and single influencing factors, such as biophysical factors [67]. Specifically in Ethiopia, there are a few studies that are spatially limited and focused on single-factor analysis [9,11,20,63] and failed to disclose the comprehensive characterization of the LST-green space nexus [9,10]. In addition, a couple of issues of great importance serve to justify our research: 1) The analyzed cities do not have enough UGS-LST interlinks studies for responses with spatial and temporal variability. 2) The study period (1990–2020) covered by this research is a positive element, allowing a view of how the indices and factors investigated vary over an extended time interval. Hence, LST dynamics and responses in green space are the result of a combination of several spatially neighboring and fundamental factors [56].

For this study, we selected the fast-growing cities in Ethiopia (Addis Ababa, Hawassa, Adama, and Bahar Dar) as study sites to filling this gap by analyzing the spatial distribution of green space, LST characteristics, spatial patterns, dynamics nexus responses to multiple influencing factors to support future climate mitigation actions and human adaptive strategies in the cities. Cities have

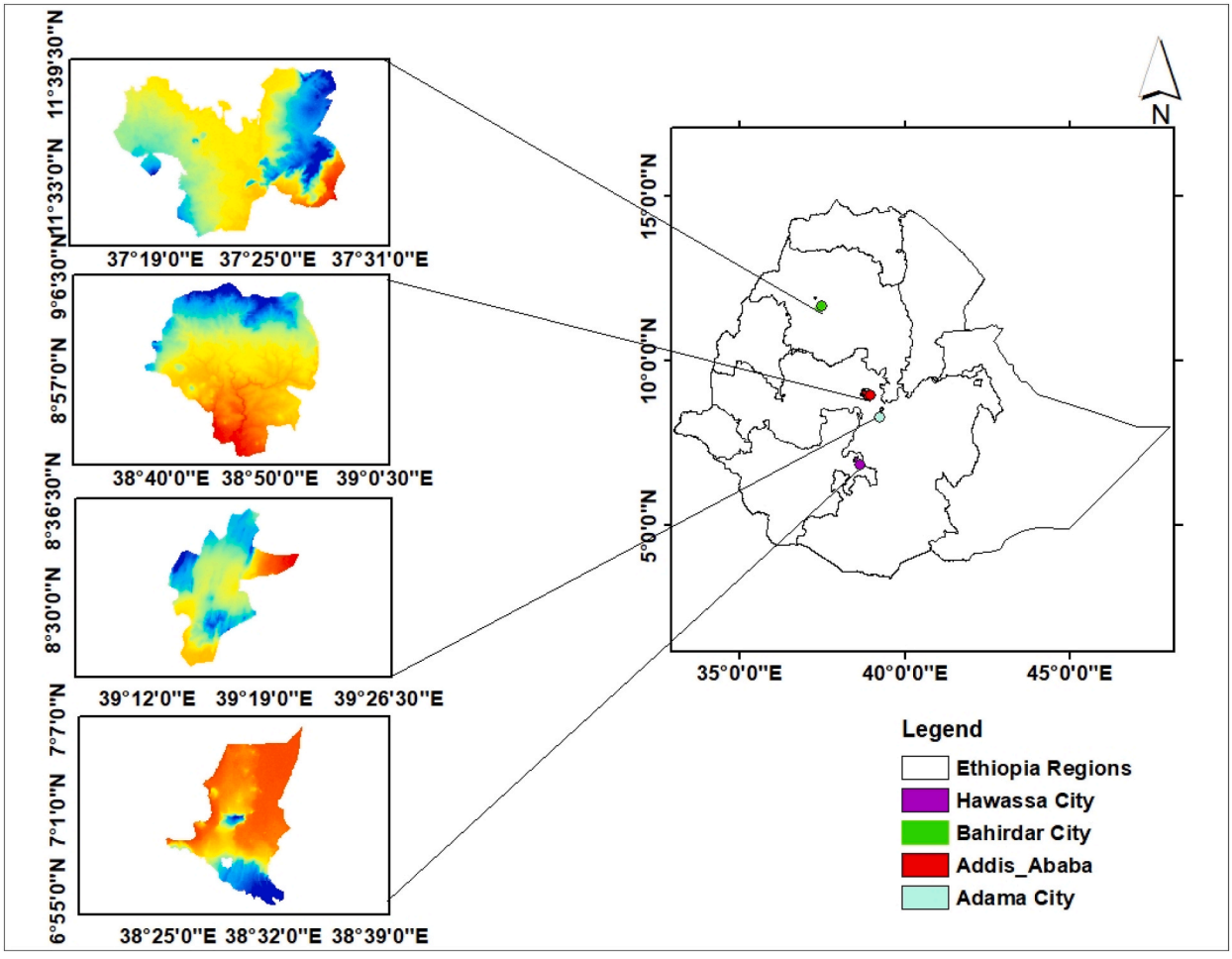

Fig. 1. Location of the study areas.

experienced massive urban construction and more rapid changes in green space. Therefore, this would be an ideal site to examine green space conversion and associated thermal effects. We conducted this study to: (1) investigate the dominant combinations of urban ecosystem dynamics in cities from 1990 to 2020; (2) quantify the spatial pattern and change of LST based on green space losses and expansion in cities; (3) model the relationships between influencing factors and LST; and (4) identify the contribution rate of each factor to UHI.

2. Materials and methods

2.1. Study areas

The study areas fall within one capital city (Addis Ababa) and three regional capital cities (Hawassa, Adama, and Bahir Dar) of Ethiopia (Fig. 1 and Table 1). The cities were identified and chosen based on the following criteria: (i) being a capital or regional city; (ii) city size and population density; (iii) being an active zone of economic and industrialization; and (iv) fulfilling the concept of the urban-rural dichotomy [8]. Additionally, the cities' elevation, location, population density, and climateic information were presented in Table 1 accordingly.

2.2. Data sources

This study uses a hybrid method to scrutinize the UHI responses to LULC dynamics by analyzing LST. This method combines the geospatial technique, Mono-window algorithm, and normalized difference vegetation index, normalized difference built-up index,and normalized modified difference water index, and is then applied to the cities of Ethiopia. For geospatial technique, we used Landsat 5 TM, Landsat 7 ETM+, and Landsat 8 OLI thermal infrared images for the retrieval of LST and production of LST maps representing four time periods of 1990, 2000, 2010, and 2020, respectively (Table 2). Furthermore, the beginning of the years LULC change and LST map generation were linked to political and policy changes in Ethiopia, which were thought to have an impact on various aspects of the country's urban development [8]. The spatial resolution of the visible and near-infrared bands of Landsat is 30 m, while the spatial resolutions of the thermal infrared bands are 120, 60, and 100 m for TM, ETM+, Landsat 8 Thermal Infrared Sensor (TIRS), respectively (http://earthexplorer.usgs.gov) and the fusion temporal enhancement method were used to reconstruct the original LST products at normalized scales in this study [11,45]. Besides, for three decades (1990–2020), LULC dynamics datasets in this study were obtained from Ref. [8].

According to Ref. [8]; after preprocessed the data, landscape classification was performed; First, an unsupervised classification technique was applied to obtain the major land use and land cover (LULC**)** types of each city, which was then used for supervised classification. Spectral signatures and ground verification using high spatial resolution imagery made available by Google Earth® in 1990, 2000, 2010, and 2020 reference data were collected, respectively for the classification of imagery in the years 1990, 2000,2010, and 2020 (Fig. 2). The reference data for each of the images was randomly split into 70% (for classification) and 30% (for accuracy assessment). Later, the landscape type class was done using the maximum likelihood classifier. In this study, the accuracy was assessed using a validation dataset obtained from historical high-resolution imagery made available by Google to assess the accuracy of classification of the current imagery (2020), Geographical Positioning System (GPS) was used to collect ground-truthing data [8]. Finally, the land use and land cover map with five illustrious classes for 1990, 2000, 2010, and 2020 and temporal deviations per city was produced and interpreted [8,10]. The five land use and land cover nomenclature (Table 3) were done according to CORINE Land Cover level 1 nomenclature [19]. Furthermore, the LULC change was culculated using Eq. 1

$$Change\ (\%) = \frac{(A_m - A_{m-1})}{A_{m-1}} * 100 \qquad \text{Eq 1}$$

2.3. Land surface temperature (LST) derived and processing

LST retrieved was from the thermal infrared band 6 and 10 of the Landsat 5–7 and 8 respective, using the single-channel algorithm

Table 1
The description of four cities (location, elevation, population, size, temperature).

Cities	Location *	Elevation range*	Projected population, size from 2007 **	Temperature (minimum & maximum)*	Rain fall per year (Average) *
Addis Ababa	8°50′00″N-9°06′00″N and 38°39′00″E–38°55′00″E	2050 m –3304 m	4,794,000	9.01 °C and 38.75 °C	1255 mm
Hawassa	7°00′30″ N-7°06′00″N and 38°28′34.86″ E–38°32′00″E	1682 m –2632 m	315,267	7.06 °C and 38.47 °C	993.4 mm
Adama	8°30′00″N-8°35′00″N and 39°13′00″E–39°18′00″E	1341 m - 2452 m	324,000	8.55 °C and 39.27 °C	804 mm
Bahir Dar	11°3′00″N–11°37′00″N and 37°20′00″E–37°26′00″E	1717m–2010 m	180,094	11.59 °C and 37.39 °C	1839 mm

Source: * [47]; ** [6].

Table 2
List of satellite data and acquisition date of the study areas.

Cities	Path/ Row	Image Acquisition Date				Bands number used for LULC	Bands number used for LST & other variables
		1990	2000	2010	2020		
Addis Ababa	168/054	04/02/ 1990[a]	05/02/ 2000[b]	31/01/ 2010[b]	29/01/ 2020[c]	1,2,3,4,5 and 7	[a,b]6 &[c]10
Adama	168/054	04/02/ 1990[a]	05/02/ 2000[b]	31/01/ 2010[b]	29/01/ 2020[c]	1,2,3,4,5 and 7	[a,b]6 &[c]10
Bahir Dar	170/052	02/02/ 1990[a]	11/02/ 2000[b]	14/02/ 2010[b]	18/02/ 2020[c]	1,2,3,4,5 and 7	[a,b]6 &[c]10
Hawassa	168/055	19/01/ 1990[a]	12/01/ 2000[b]	31/01/ 2010[b]	19/01/ 2020[c]	1,2,3,4,5 and 7	[a,b]6 &[c]10

[a] Landsat TM: [b]Landsat ETM+:[c]Landsat OLS.

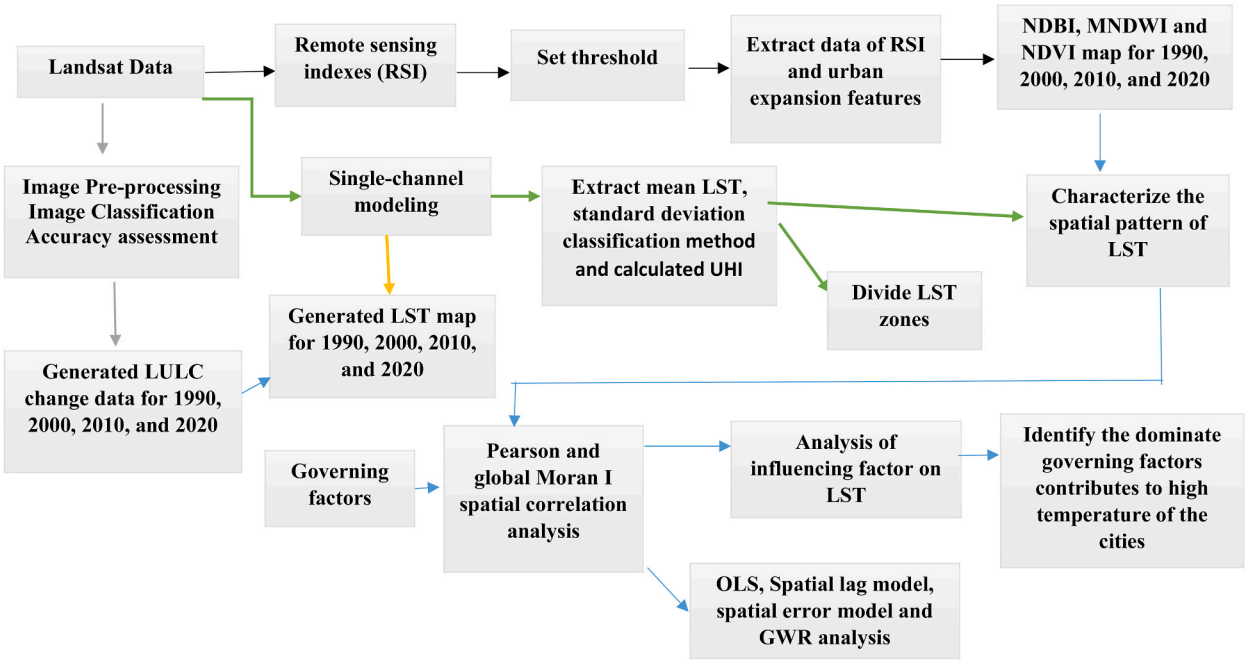

Fig. 2. Flow chart of methodological approach.

Table 3
Types of LULC and its description.

LULC type	Description[a]
Urban forest and greenery (UFG)	Areas occupied by plantation forest and urban green parks with 65% canopy cover or higher, evergreen and mixed urban forests and greenery and other vegetation that is relatively tall and dense, as well as areas covered with both indigenous and exotic trees.
Urban agriculture (UA)	The purpose is used for urban crop production and livestock husbandry grazing land by peri-urban field farmers, although cultivated land use is relatively different in terms of size, soil fertility, use of input, and other important variables from rural agriculture. Includes, grazing areas, cultivated lands, community open lands, and areas along the lakeshore that are used for agricultural purposes when the lake level retreats following the long dry-season.
Water bodies (W)	Permanent natural water bodies such as lakes, rivers, pond reservoirs, and man-made water bodies, the water table in irrigated land.
Built-up (BU)	The built-up area with congested buildings includes all types of artificial surfaces, residential and scattered settlements in urban fringe zones, commercial, industrial land uses as well as transportation infrastructure.
Bare land (BL)	The land consists of roads, rocky outcrops, and degraded lands, where the area is dominated by the regular movement of trucks, quarry for road construction, and abandoned lands as a result of gully formation, etc.

[a] Adopted from the standard CORINE Land Cover level 1 nomenclature [19].

[2,37]. First, the digital numbers were converted into absolute radiance using Eq (2) [53]. Accordingly, the TOA radiance of the thermal band was transformed into at-sensor brightness temperature using Eq (3) [9,11,39].

$$L_{\lambda} = \frac{(L_{max} - L_{min})}{255 * DN + L_{min}} \quad \text{Eq 2}$$

where L_{λ} is the spectral radiance, L_{min} and L_{max} (mW/(cm^2.sr.μm)) are spectral radiances for each band at digital numbers 0 and 255, respectively. For TM 5, Lmin and Lmax were the values 0.124 and 1.530 in (mW/(cm^2.sr.μm)), respectively.

$$T_B = \frac{K_2}{\ln\left(\frac{K_1}{L_{\lambda}} + 1\right)} \quad \text{Eq 3}$$

Where T_B is the at-sensor brightness temperature in Kelvin; L_{λ} equals TOA radiance and $K_1 = 607.76$ W/(m^{2}sr μm) and $K_2 = 1260.56$ W/(m^2.sr.μm) are pre-launch calibration constants.

The generated brightness temperature values (Eq (2)) were then converted to emissivity-corrected LST in Kelvin using Eq (3). Furthermore, study areas are heterogeneous areas; thus, to avoid the emissivity effect (ε) in estimating LST, the NDVI threshold method was applied using Equations (4–7) [9,13].

$$LST = \frac{T_B}{1 + \left(\lambda * \frac{T_B}{\alpha}\right) \ln \varepsilon} \quad \text{Eq 4}$$

Where λ is the wavelength of emitted radiance equals 11.5 μm; α = hc/b (1.438 × 10ˆ-2 mk); b refers to Boltzman constant as 1.38 × 10ˆ-23 J/K; h is the Planck's constant 6.626 × 10ˆ-34 JS; C refers to the velocity of light 2.998 × 10ˆ8 m/s, and ε is the surface emissivity.

$$\varepsilon_{mix} = \varepsilon_v p_v + (1 - p_v) + C_i \quad \text{Eq 5}$$

$$p_v = \left(\frac{NDVI - N\ DVI_{min}}{NDVI_{max} - N\ DVI_{min}}\right)^2 \quad \text{Eq 6}$$

$$C_I = (1 - \varepsilon_n)(1 - P_v)F \quad \text{Eq 7}$$

Where $\varepsilon_v = 0.985$ and $\varepsilon_n = 0.92$ (urban surface) [50]; NDVI max and NDVI min are the values of full vegetation and non-vegetation respectively; Pv is the scaled NDVI/fractional vegetation cover; and F = 0.55, which refers to the shape factor for geometric distribution. To this end, the calculated temperature in Kelvin is then converted into centigrade for ease of interpretation using Eq (8).

$$LST = \frac{K_2}{\ln\left[\left(\frac{K_1}{L_T}\right) + 1\right]} - 273.15 \quad \text{Eq 8}$$

where K1 = 607.76 W/(m2 *sr*μm), and K2 = 1260.56 K in Landsat TM; K1 = 666.09 W/(m2 *sr*μm), and K2 = 1282.71 K in Landsat ETM+; and K1 = 774.89 W/(m2 *sr*μm), and K2 = 1321.08 K in Landsat 8 TIRS [24,29].

LST data was normalized (Eq (9)), which could remove deviations of the extracted temperature outcomes caused by different imaging times and excavate sympathetic of development patterns of land surface temperature evolution [51,66]. Furthermore, the normalized LST was grouped into low-temperature region (T < Mean-STD), middle-temperature region (Mean-STD < T ≤ Mean − 0.5STD), and high-temperature region (T > Mean + STD) according to mean - standard deviation (STD) classification methods [2,9].

$$N_i = \frac{LST_i - LST_{min}}{LST_{max} - LST_{min}} \quad \text{Eq 9}$$

2.4. Extraction and compute remote sensing indexes in cities

To analyze, the influence of remote sensing indexes on LST dynamics; normalized difference vegetation index (NDVI), normalized difference built-up index (NDBI), and modified normalized difference water index (MNDWI) were computed from surface reflectance to represent urban ecosystem dynamics [25,65]. NDVI has been widely used to represents the proportion of the vegetative (green) surface cover and calculated from the near-infrared and red bands using Eq (10). The MNDWI is computed to extract open water features using Eq (11). Hence, it is more accurately extracts open water features than the MNDWI in the urban ecosystem [56,61]. On the other hand, the NDBI is calculated to identifying built-up landscapes from medium resolution satellite imagery. It is derived using the surface refectance of SWIR1 and NIR band (ρSWIR1 and ρNIR) of Landsat 5 TM (bands 5 and 4) and Landsat 8 OLI/TIRS satellite sensor (bands 6 and 5) [56,61] using Eq (12).

$$NDVI = \frac{(\rho NIR - \rho RED)}{(\rho NIR + \rho RED)} \quad \text{Eq 10}$$

$$\mathrm{MNDWI} = \frac{(\rho\mathrm{Green} - \rho\mathrm{MIR})}{(\rho\mathrm{Green} - \rho\mathrm{MIR})} \quad \text{Eq 11}$$

$$\mathrm{NDBI} = \frac{(\mathrm{SWIR_1} - \mathrm{NIR})}{(\mathrm{SWIR_1} - \mathrm{NIR})} \quad \text{Eq 12}$$

Where: NIR is the near-infrared band, Red is a red band, Green is a green band, SWIR1 is the short-wave infrared band. MNDWI ranges from −1 to 1, and positive values represent water bodies.

2.5. Urban heat island calculation

The urban heat island (UHI) is the key area for urban planning and management aims. Human influences and population pressure have increased land dynamics and thermal variation [11,23,26]. Urban Heat Islands (UHIs) characterize as dense urban areas within cities where the temperature is recorded to be higher than the neighboring areas or those located in suburbia [9,11,48]. Surface urban heat island (SUHI) and canopy urban heat island (CUHI) are mostly research concerns which aim to identify the thermal variation and ecological disturbances of the earth's surface [9,27]. For the appraisal of urban thermal balance, it is essential to estimate the intensity of UHIs [21,26]. For UHI calculations, LST data from satellite image calculations was used. The UHI in the cities is estimated to use Eq. (13).

$$UHI = \left(\frac{LST_{pixel} - LST_{mean}}{SD}\right) \quad \text{Eq 13}$$

where $\mathrm{LST_{pixel}}$ indicates the values of the pixel, $\mathrm{LST_{mean}}$ indicates the mean LST of the area in study, and SD indicates the standard deviation of the calculated LST map.

2.6. Correlation and spatial regression analysis

Land surface temperature (LST) can be influenced by many factors, such as urbanization, environment, and economy [61]. In this study, seven influencing factors were considered from three perspectives of geographic location ($\mathrm{X_{1:\ Latitude,}}$ $\mathrm{X_{2:\ Longitude,}}$ $\mathrm{X_{3:\ Altitude}}$), remote sensing index (NDVI, NDBI, NMDWI), and population density factors. The correlation coefficient between different factors and LST was calculated through Eq. (14). In this study, the global Moran's I index was also used to describe the global cluster characteristics of the value of LST using Eq (15). Besides, the spatial regression analysis was applied to study the spatial dependence of LST on influencing factors using the ordinary least squares (OLS) model, spatial lag model (SLM), spatial error model (SEM), and geographically weighted regression (GWR) using Eq. (16) and (17) [4,42,70]. The Moran's I analysis, OLS, and SRMs, were investigated using GeoDa 095i. While the GWR model was analyzed using GWR 4.0 software [4].

$$rp^{i,j} = \frac{\sum_{k=1}^{m}(X_{ik} - x_i)(X_{jk} - x_j)}{\sqrt{\sum_{k=1}^{m}(X_{ik} - x_i)^2 \sum_{k=1}^{m}(X_{jk} - x_i)^2}} \quad \text{Eq 14}$$

where rp (i, j) is the correlation coefficient; Xik and Xjk are numerical values of different factors and LST; Xi and Xj are means of different factors and LST, respectively; and m is the number of pixels.

$$\mathrm{Moran's\ I} = \frac{\mathrm{n}\sum_{i=1}^{n}\sum_{j=1}^{n}(x_i - \bar{x})x_j - \bar{x})}{\sum_{i=1}^{n}\sum_{j=1}^{n}W_{ij}\sum_{i=1}^{n}(x_i - \bar{x})} \quad \text{Eq 15}$$

Where x_i and x_j are the variable values of units i and j, $\bar{x}$ is the mean of variable x; and W_{ij} is the spatial weight matrix. The values of Moran's I range from −1 to 1.

$$Y = \rho WY + X\beta + \varepsilon \quad \text{Eq 16}$$

$$Y = X\beta + \lambda W\mu + \varepsilon \quad \text{Eq 17}$$

Where, Y is the N-by-1 vector of dependent variables: X is the N-by-M matrix of independent variables (NDVI, NDBI, and MNDWI values and constants) and β is the corresponding regression coefficient matrix. μ and ε are spatially autoregressive error terms and random error terms, respectively. ρ and λ are spatial lag terms and spatial error terms, respectively. W is a spatial weight matrix.

3. Results

3.1. Landscape features dynamics and variation of LST in cities

Fig. 3 shows the growth of the built areas of each city in 1990, 2000, 2010, and 2020. In all the cities, the built area has expanded unceasingly from 1990 to 2020. The built area in Addis Ababa was 12606.9ha, 14564.5ha, 18653.5ha, and 29947.9ha in 1990, 2000, 2010, and 2020, sequentially. Adama was followed in terms of expanded area ratio (Fig. 3b). The built area in Adama was 1723.77ha, 2125.44ha, 2279.16 ha, and 3875.04ha in the years 1990, 2000, 2010, and 2020, respectively. It was augmented by 2151.27ha (19.64%) from the initial study period. The built area in Hawassa was 1072.62ha in 1990. The city's fringe zone was increased to 3672.27ha by 2020 and overall prolonged by 2599.65ha (15.71%) within the last three decades (Fig. 3c). Besides, the built area coverage of Bahir Dar was 2087.91ha, 2609.73ha, 2966.67ha, and 4803.12ha in the years 1990, 2000, 2010, and 2020, respectively (Fig. 3d). In general, the urbanization of Bahir Dar was augmented by 2715.21ha (12.72%) from 1990 to 2020 (Fig. 4).

Overall, the LST patterns and trends of each city from 1990 to 2020 have an analogous flow to urbanization dynamics (Fig. 3a–d). The mean LST for 2020 was the highest in Hawassa (36.6 °C), while it was the lowest in Addis Abeba (26.14 °C) in 1990. Moreover, Fig. 6 shows the UHI values of each city for different time periods. The lowest and highest UHI values in Adam are 2.24 (2000) and 2.89 (2020); in Addis Abeba, 2.98 (2020) and 3.74 (1990); in Bahir Dar, 2.24 (2020) and 2.98 (1990); and in Hawassa, 2.64 (1990) and 3.58 (2020), respectively. This result indicates the effect of UHI in each city, where urban expansion and low green space are the main reasons for this variation.

3.2. Spatiotemporal characteristics of LST and remote sensing indexes

The spatiotemporal features of the LST in each city are revealed in Fig. 5. While the LST values were not strictly analogous across cities, since each city varies in terms of spatial extent and development endeavors, Thus, the general characteristics of LST would show the synoptical patterns of the cities. Bahir Dar had a three-decade mean LST range of 28.28–34.52 °C, Addis Ababa had a range of 26.07–29.01 °C, Hawassa had a range of 25.02–28.84 °C, and Adama had a range of 28.24–32.88 °C (Fig. 6).The frequency distributions of LST were slightly left-skewed in each of the four cities. The frequency distributions of NDVI, MNDWI, and NDBI values were right- and left-skewed, respectively, for all four cities (Fig. 7). However, NDVI and NDBI values were significantly different among the cities. The mean value range of NDVI in Bahir Dar (−0.19-0.20), Addis Ababa (−0.18-0.14), Hawassa (0.04–0.27), and Adama (−0.20-0.16). While the mean NDBI varied within the range in Bahir Dar (−0.076), Addis Ababa (0.01–0.23), Hawassa (−0.06-0.23), and Adama (0.06–0.27). In addition, the mean MNDWI result shows a negative value in all years for each city (Fig. 7).

Fig. 3. Urbanization changes in 1990, 2000, 2010, and 2020 for (a) Addis Ababa, (b) Adama, (c) Hawassa, and (d) Bahir Dar.

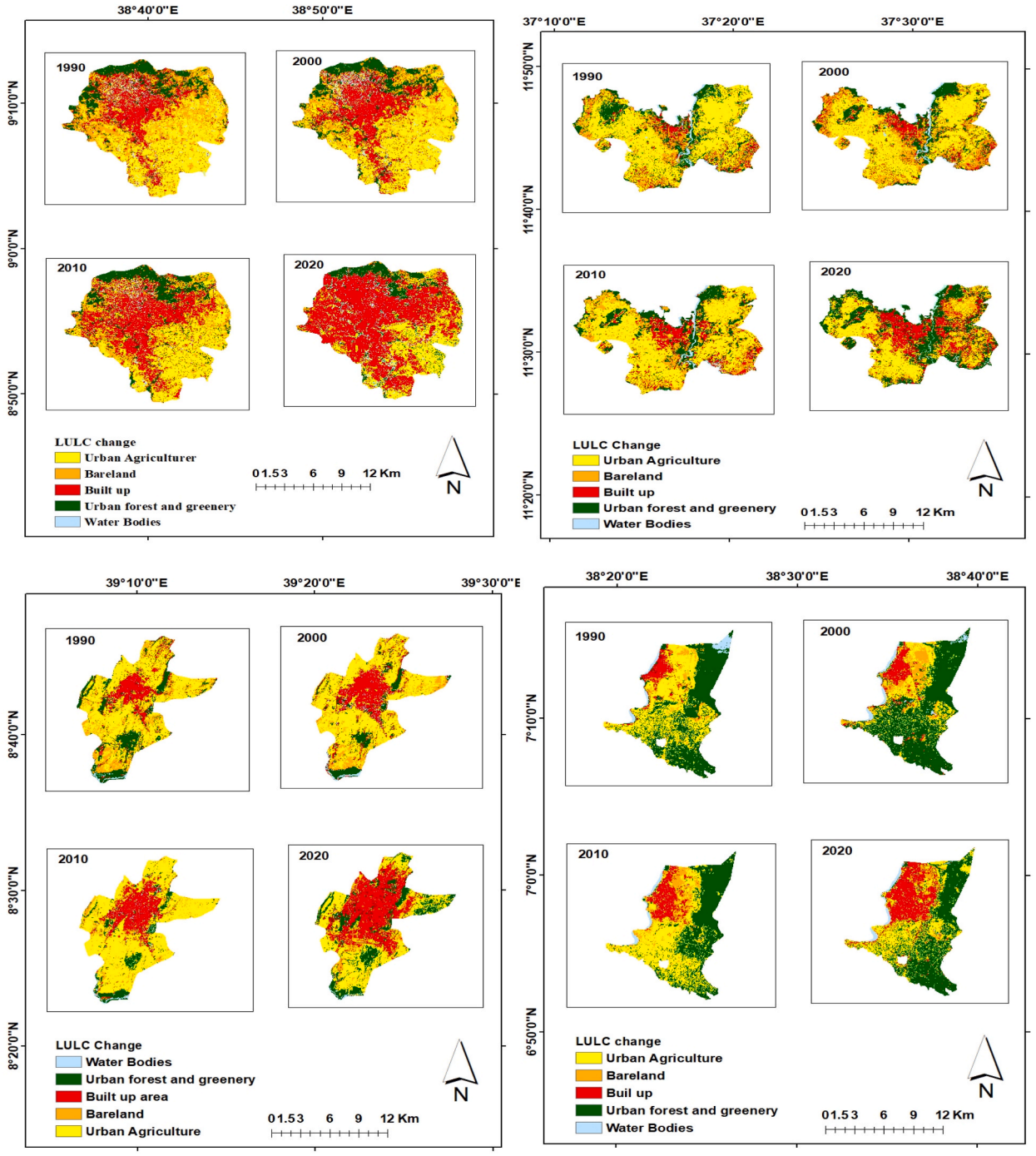

Fig. 4. Spatial distribution of LULC change in (a) Addis Ababa, (b) Bahir Dar, (c) Adama, and (d) Hawassa cities respectively.

The spatial pattern of LST of the four cities of 1990, 2000, 2010, and 2020 is shown in Fig. 8. The finding shows that in 1990, high-temperature zones were relatively concentrated in residual areas, markets, government, industry areas, and non-government infrastructures, with low urban forest and greenery cover landscapes (Fig. 4). The high-temperature zones of Addis Ababa were found in the southwest part and covered 6169.8ha, for Adama intensified in the northeast and accounted for 1145.25ha, Bahir Dar dominated the center of the city and sparked in all directions and enfolded 1606.06ha, and Hawassa covered 3234.33ha and was found in the center and northwest parts of the city. Middle-temperature zones in each city covered a range of 3–7 folds that of high-temperature zones, and the distribution was relatively uniform in all directions, whereas low-temperature regions are primarily concentrated at city boundaries and mountains (Fig. 8).

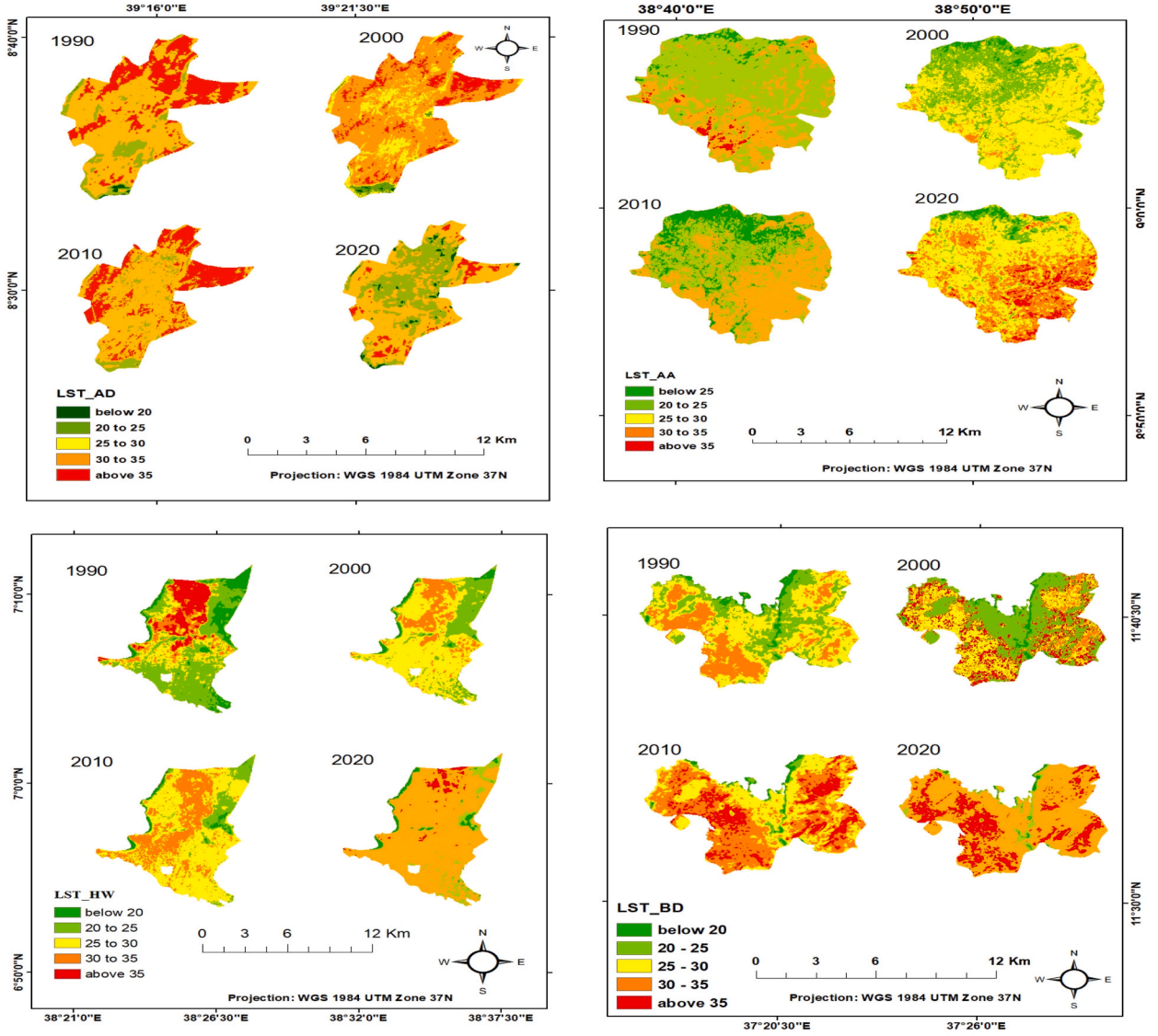

Fig. 5. Remotely sensed LST of each city for 1990, 2000, 2010, and 2020.

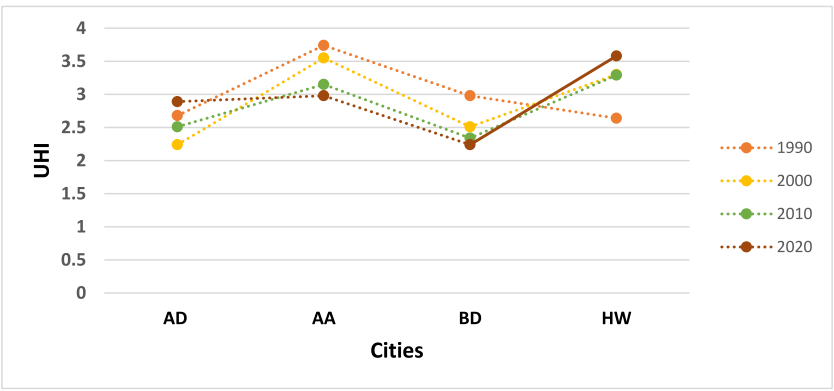

Fig. 6. The urban heat island (UHI) difference between UGS and non UGS areas.

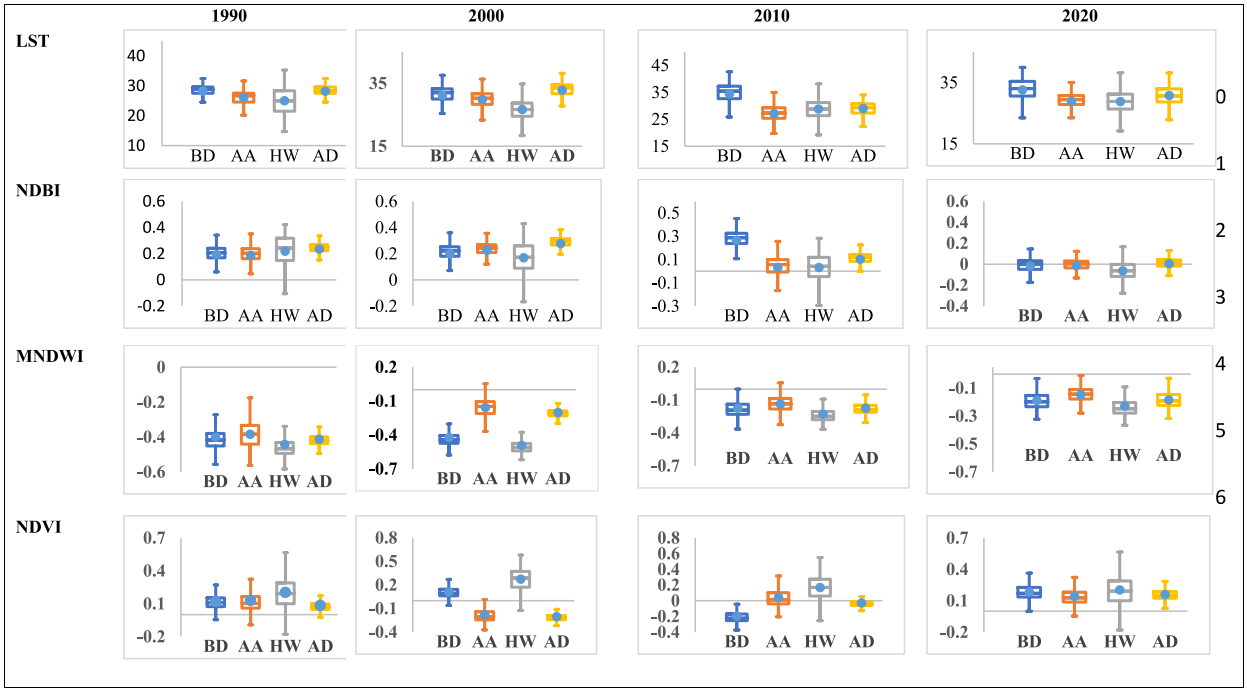

Fig. 7. Boxplots of LST and remote sensing indexes in four cities. AA, AD, BD, and HW represent Addis Ababa, Adama, Bahir Dar, and Hawassa, respectively.

At the end of study period (2020), the spatial distribution of LST will have significantly changed in all cities. The proportion of high-temperature regions in Addis Abeba has decreased by 2773ha since 2010, with the spatial concentration concentrated in the city's northeast and southeast.Similarly, the area of low-temperature regions decreased. By contrast, middle-temperature regions had increased (Fig. 8c and d). The distribution of high-temperature regions in Bahir Dar was concentrated on the western part of the Abay River (Blue Nile) and spatial coverage was increased by 2168.31ha from 2010. Furthermore, the spatial pattern of low-temperature areas was altered, with water bodies, urban forests, and greenery dominating.Furthermore, Adama (Fig. 8a) demonstrated the expansion of high-temperature regions in all directions of the outskirts of the city and increased the evolution by 606.33ha from 2010 at the cost of the middle-temperature area. While the high-temperature regions of Hawassa were relatively stable in the past two decades and were spatially concentrated in the northern part of the city, In general, the spatial and temporal evolution rates of LST in the selected cities varied from city to city during the 1990s–2020, and the rate and coverage were higher in Addis Ababa and Adama (Fig. 8a–d).

3.3. Influencing feature factors on LST dynamics

The Pearson correlation analysis between LST and inducing factors ($p < 0.05$) is presented in Table 4. The finding shows that LST had a positive correlation with NDBI and substantially contributed to the heating effect. Furthermore, Hawassa revealed the highest correlation coefficient of 0.85 in 1990, followed by Addis Ababa and Adama, showing a strong correlation coefficient of 0.73 in 2010 and 2000, respectively. While Addis Ababa, Adama, and Bahir Dar found moderate correlation coefficients of LST with NDBI of 0.55, 0.48, and 0.67 in 2020, respectively. In contrast, all cities exhibited a low to moderate negative correlation between LST and MNDWI (0.16–0.60) in the past three decades. The MNDWI and LST had a moderate negative correlation in Hawassa (0.50–0.55) and Bahir Dar (0.43–0.54), but the weakest correlation was found in Addis Abeba, ranging from 0.13 to 0.33 during the study period. Furthermore, negative moderated correlations were detected between LST and NDVI with a range of 0.29 to 0.64 in all cities. Conversely, the relationship between LST and geographical location and population density factors varied among cities through the time change. In 1990, LST was positively correlated with longitude factors in Adama and Hawassa but negatively correlated with longitude in Bahir Dar and Addis Abeba ($p < 0.05$). Hence, cities are found in different climate regions. Besides, Addis Ababa showed moderated negative correlations between LST and altitude, with correlation coefficients being 0.58 and 0.46 in 1990 and 2020, respectively. While LST in Bahir Dar shows the lowest negative significant correlation (0.21) with altitude in 1990, Adama and Addis Ababa were positively correlated to population density in 1990, 2010, and 2020, respectively (Table 4).

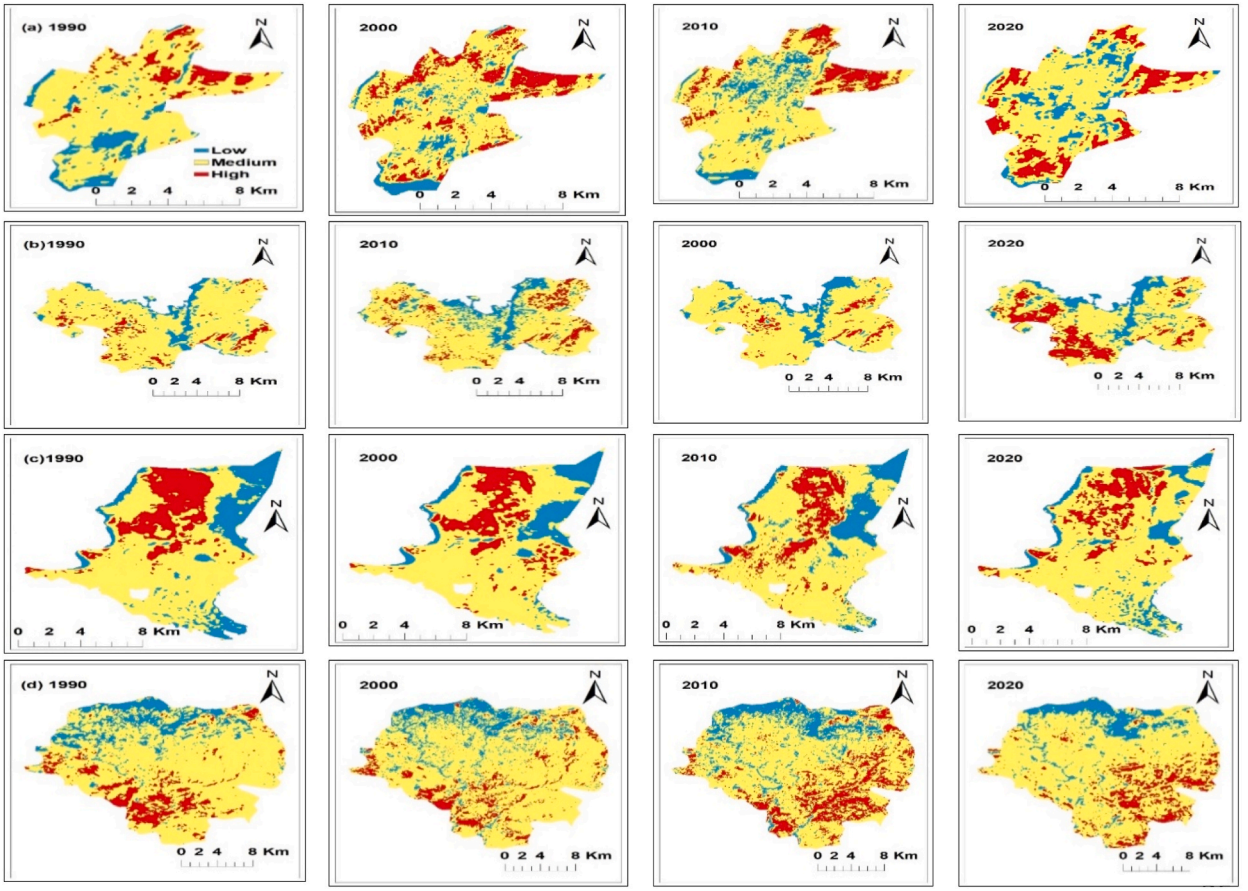

Fig. 8. Spatial distribution of LST in 1990, 2000, 2010, and 2020 for (a) Adama, (b) Bahir Dar, (c) Hawassa, and (d) Addis Ababa.

Table 4
Correlation coefficient between LST and influencing factors per years.

City/year	X1	X2	X3	X4	X5	X6	X7
Hawassa							
1990	0.31	0.13	−0.30	0.00	**0.85**	**−0.55**	**−0.59**
2000	0.22	0.33	0.21	0.00	**0.80**	**−0.52**	**−0.50**
2010	0.32	0.11	0.21	−0.21	**0.84**	**−0.50**	**−0.54**
2020	0.20	0.12	0.10	−0.11	**0.56**	**−0.50**	−0.42
Addis Ababa							
1990	−0.12	**−0.55**	**−0.58**	−0.21	**0.61**	−0.16	**−0.59**
2000	−0.11	0.21	0.31	0.00	**0.65**	−0.13	**−0.63**
2010	−0.21	0.00	−0.23	0.00	**0.73**	−0.30	**−0.64**
2020	0.20	0.00	−0.46	0.41	**0.55**	−0.33	−0.44
Bahir Dar							
1990	−0.13	−0.18	−0.21	0.13	**0.62**	−0.44	−0.26
2000	−0.06	−0.25	0.00	0.02	**0.67**	−0.46	−0.34
2010	−0.06	−0.17	0.11	0.02	**0.62**	−0.43	−0.48
2020	−0.17	−0.32	0.00	0.01	**0.66**	**−0.54**	−0.41
Adama							
1990	−0.19	0.48	−0.22	0.11	**0.62**	−0.40	**−0.54**
2000	−0.15	0.34	0.17	0.21	**0.73**	−0.41	**−0.63**
2010	−0.10	0.26	0.00	0.32	**0.65**	−0.30	−0.46
2020	−0.04	−0.17	0.12	0.00	0.48	−0.20	−0.19

The significance of bold is that the correlation coefficients between LST and factors are higher than 0.50 X_1: Latitude, X_2: Longitude, X_3: Altitude, X_4: Population density, X_5: NDBI, X_6: MNDWI, X_7: NDVI, X_8: LST.

3.4. Spatial correlation and dependence of LST on remote sensing indexes

3.4.1. Global bivariate Moran's I and spatial regression models

Table 4 illustrates the global bivariate Moran's I result are positively spatial correlations between LST and NDBI, while negatively correlated with MNDWI and NDVI (p-values <0.001). Moreover, the rate of urban agglomeration causes an upsurge in LST and UHI intensities. Thus, the magnitude of correlation ranged between −0.07 and 0.76, and varied with remote sensing indexes and among cities (Table 5). A positive moderate spatial correlation was found between LST and NDBI (Moran's I: 0.76 and 0.43 for Addis Ababa and Adama respectively. The weakest positive correlation was observed between LST and NDBI (Moran's I: 0.07 and 0.12) for Bahir Dar and Hawassa respectively, in 2020. In contrast, a negative moderate spatial correlation was reported between LST and MNDWI (Moran's I: 0.24) for Adama, followed by that between LST and NDVI (Moran's I: 0.38 and 0.24) for Adama and Addis Ababa, respectively (Table 5). The weakest negative correlation was found between LST and NDVI and MNDWI (Moran's I range with 0.10–0.16) of the selected cities.

3.4.2. Multivariate analysis of governing factors on LST dynamics

The OLS (SLM or SEM) results indicate that spatial dependence occurs in all regressions ($p < 0.01$), the variance inflation factor (VIF) was <5 and there were no multicollinearity problems in the explanatory variables (Table 5). Therefore, the SEM was used for Adama, Bahir Dar, and Hawassa cities, whereas the SLM was selected for Addis Ababa (Table 5). Moreover, OLS regression reveals that the effect of controlling factors on LST is generally small, hence influencing variables mostly affect LST concurrently. Furthermore, in Adama and Addis Ababa, NDBI has significantly controlled the spatial pattern of LST, and its coefficient in the OLS was 3.1 and 2.06 in 2020 respectively, followed by NDVI > MNDWI > latitudes > longitude > population density > DEM. While in Hawassa and Bahir Dar, MNDWI was substantially controlled by LST change, and its coefficient in 2020 was 2.56 and 2.0 and followed the NDVI/NDBI > NDBI/NDVI > latitudes > longitude > population density > DEM pattern, respectively (Table 5).

Table 6 shows that the OLS regression disparities of LST in the same city but in different years. The results revealed that the ranges of negative coefficient values of MNDWI were the leading factors for Bahir Dar and Hawassa from 1990 to 2020 with 1.92–3.07 and 1.56–2.56, respectively. This shows that although the coefficient of MNDWI changed in different years, its influence on LST remained significant ($p < 0.01$). In Bahir Dar, the coefficient of NDVI was highest in 2000; it was the lowest in 2020. Besides, in Hawassa, the coefficient value of the NDVI was the dominant factor in 2020, while it was the lowest in 2010. The determinant factor NDBI was the most important variable in 2020 and 2010 for Bahir Dar and Hawassa, respectively. In Addis Ababa, the principal influencing factor was NDVI, with the ranges between 0.99 and 1.98 of regression coefficients from 1990 to 2020. Besides, NDBI was the highest determining factor, with a value of 3.1 in 2020. In contrast, in all city development stages, the coefficient that determines the value of NDBI was dominant in Adama, with regression coefficients ranging from 0.12 to 2.06 (Tables 4 and 5). This infers that "high or low" of the coefficient of an inducing factor is only associated with the comparative importance of the influencing factor in the OLS regression analysis in a specific year. Nevertheless, MNDWI, NDBI, and NDVI ranked high in all developmental stages of the years of each city in terms of the regression coefficients, showing that the change in water content, urban pattern, surface albedo intensity, evapotranspiration, and heath of greenery were principally affecting the spatial-temporal distribution and magnitude of UHI (Tables 5 and 6).

The magnitude and direction of the regression coefficients of the influencing factors changed significantly during urban expansion. However, the dominant controlling factor on LST did not change significantly. For example, NDBI was the dominant controlling factor on LST for Addis Ababa in 1990, 2010, and 2020, and the coefficient sign was positive, demonstrating the positive effect of NDBI on LST, i.e., LST increased with the expansion of urbanization, while in 2000 the coefficient sign was negative, demonstrating the cooling effect of NDVI and MNDWI on LST (Table 6 and Figs. 4–5). On the other hand, MNDWI and NDVI were the dominant controlling factors on LST for all cities from 1990 to 2020, and the sign was negative for all years except Adama in 2020 (MNDWI), which does not significantly affect LST dynamics (Table 6 and Figs. 4–5). Besides, the sign of the coefficients of other factors on LST changed with time but was not significantly correlated ($P < 0.05$) to LST, indicating their minimal influence on LST (Table 7).

3.4.3. LST sensitivity to urban remote sensing indexes

Table 6 also shows the sensitivities of LST to remote sensing indexes resulting from OLS regressions from 1990 to 2020. These sensitivities manifested as an increase (+) or decrease (−) in the magnitude of LST with every 0.1 upsurge in given factors, which

Table 5
Global Bivariate Moran's I between LST and remote sensing indexes.

Variables	HW			AD		
	Moran's I	p-value	z-Value	Moran's I	p-value	z-Value
NDBI	0.12	<0.001	3.66	0.43	<0.001	9.59
MNDWI	−0.15	<0.001	−4.30	−0.24	<0.001	1.85
NDVI	−0.12	<0.001	−1.57	−0.38	<0.001	3.35
	BD			**AA**		
NDBI	0.07	<0.001	5.93	0.76	<0.001	15.04
MNDWI	−0.16	<0.001	−5.15	−0.10	<0.001	−9.58
NDVI	−0.14	,<0.001	−3.89	−0.24	<0.001	−13.75

Table 6
OLS regression of LST and governing factors of cities in 2020.

City	Fitting equation of OLS regression	Model	W_Y_LST/Lambda	R^2
Addis Ababa	LST = −0.01*X_1^a-0.03*X_2-0. 07*X_3-0.04*X_{4+}**3.1***X_5^a-1.01*X_6^a-1.24*X_7^a +19.35	SLM	0.34	0.49
Adama	LST = 0.03*X_1-0.24*X_2^a+0.04*X_3+0.03*X_4+**2.06***X_5^a-0.23*X_6^a+1.16*X_7^a +30.79	SEM	0.14	0.40
Hawassa	LST = 0.03*X_1+0.01*X_2-0.04*X_3-0.03*X_4^a-0.84*X_5^a-**2.56***X_6^a-2.40*X_7^a+28.84	SEM	0.14	0.64
Bahir Dar	LST = −0.6*X_1-0.076*X_2^a+0.6*X_3+0.3*X_{4+}1.23*X_5^a-**2***X_6^a-1.37*X_7^a+32.67	SME	0.04	0.61

W_Y_LST: spatial lag termof LST equation, LAMBDA: spatial error termof LST equation, a; Statistically significant at 1% level.
X_1: Latitude, X_2: Longitude, X_3: Altitude, X_4: Population density, X_5: NDBI, X_6: MNDWI, X_7: NDVI, X_8: LST.

Table 7
OLS model of LST-independent variables in different years of selected cities.

City	Year	Fitting equation of OLS regression	SLM (W_Y_LST)	R^2	SEM (LAMBDA)	R^2
BD	1990	LST = 0.18X_1-**0.42X_2^a**+0.07X_3^a+0.3X_4-**0.17X_5-1.92X_6^a-1.58X_7** +28.3	0.00	0.52	0.01	**0.53**
	2000	LST = **0.3X_1^a-0.53X_2^a**+0. 02X_3+0.03X_4-**0.37X_5-2.88X_6-2.4X_7^a** +31.26	0.02	0.61	0.03	**0.62**
	2010	LST = **0.4X_1-0.39X_2**+0.02X_3+0.3X_4-**1.15X_5^a-3.07X_6^a-2.29X_7^a**+34.5	0.01	0.56	0.03	**0.57**
	2020	LST = −0.6X_1-**0.76X_2^a**+0.6X_3+0.3X_{4+}**1.23X_5^a-2.1X_6^a-1.37X_7^a**+32.67	0.03	0.60	0.04	**0.61**
HW	1990	LST = 0.06X_1+0.8X_2+0. 05X_3^a-**0. 05X_4^a+0.19X_5^a-2.05X_6^a-2.2X_7^a** +25.03	0.08	0.75	0.18	**0.76**
	2000	LST = 0.03X_1+0.2X_2-0.03X_3^a-0.3X_4+**0.9X_5^a-1.57X_6^a-1.45X_7^a** -26.7	0.04	0.67	0.10	**0.68**
	2010	LST = 0.02X_1-0.01X_2-0.01X_3-0.04X_4^a+**1.59X_5^a-1.56X_6^a-1.24X_7^a** +29.54	0.05	0.74	0.10	**0.74**
	2020	LST = 0.03X_1+0.01X_2-0.04X_3-0.03X^a4-**0.84X_5^a-2.56X_6^a-2.40X_7^a**+28.84	0.07	0.61	0.14	**0.64**
AA	1990	LST = 0.47X_1-**0.62^{a}X$_2$-0.5X_3^a**-0.4X_4+**0.17X_5-0.86X_6^a-0.99X_7^a**+26.07	−0.01	0.58	−0.01	**0.59**
	2000	LST = −0.002X_1-0.03X_2+0.02X_3-0.07X_4-**0.09X_5^a-1.2X_6^a-1.98X_7^a** +29.90	0.17	0.53	0.19	**0.54**
	2010	LST = −0.4X_1^a+0.57X_2-**0.08X_3**+0.04X_4^a+**0.44X_5^a-1.03X_6^a-1.76X_7^a**+27.65	0.21	**0.61**	0.22	0.60
	2020	LST = −0.01X_1^a-0.03X_2-0. 07X_3-0.04X_{4+}^a**3.1X_5^a-1.01X_6^a-1.24X_7^a** +19.35	0.34	0.49	0.33	0.48
AD	1990	LST = −0.07X_1+**0.63X_2^a**+0.18X_3^a+0.03X_4+**0.12X_5^a-0.61X_6^a-0.69X_7^a**-28.25	0.06	0.53	0.17	**0.55**
	2000	LST = 0.01X_1+**0.49X_2^a**+0. 6X_3^a+0.03X_4+**1.8X_5^a-0.99X_6^a-1.22X_7^a**-32.9	0.05	0.60	0.09	**0.61**
	2010	LST = −0.01X_1+0.45X_2-**0.08X_3**+0.03X_4+**0.40X_5^a-1.56X_6^a-1.06X_7^a** -29.05	0.07	0.54	0.12	**0.55**
	2020	LST = 0.03X_1-**0.24X_2^a**+0.04X_3+0.03X_4^a+**2.06X_5^a**-0.23X_6^a-**1.16X_7^a** +30.79	0.13	0.39	0.14	0.40

BD: Bahir Dar, HW: Hawassa, AA: Addis Ababa, and AD: Adama.
X_1: Latitude, X_2: Longitude, X_3: Altitude, X_4: Population density, X_5: NDBI, X_6: MNDWI, X_7: NDVI, X_8: LST.

varied with city and year. For example, in Bahir Dar, LST sensitivities to NDVI was nigativly increased from 1.37 °C to 2.40 °C; in Hawassa, from 1.56 °C to 2.56 °C; in Addis Abeba, from 0.99 °C to 1.98 °C; and in Adama, from 0.19 °C (not significant) to 0.1.22 °C. LST sensitivities to MNDWI ranged from −1.92 °C to-3.07 °C in Bahir Dar, −1.24 °C to-2.40 °C in Hawassa, −0.99 °C to-1.98 °C in Addis Abeba, and −0.19 °C to-1.22 °C in Adama between 1990 and 2020. It indicated that the small presence of water bodies had an insignificant cooling effect in Addis Ababa and Adama cities, whereas their large presence had a strong cooling effect that could acutely decrease LST, in addition to the offsetting effect of urban forest and greenery found in Bahir Dar and Hawassa (Table 7). In contrast, the LST sensitivities to NDBI were the strongest in Addis Ababa (3.1 °C) in 2020, followed by Adama (2.06 °C) in 2020, Hawassa (2.16 °C) in 2010, and Bahir Dar (1.23 °C) in 2020, while they varied with the year in each city (Table 7).

3.5. Comparison of OLS model and GWR model

The evaluation of the fitting consequence between the GWR model and the OLS model is shown in Table 8. The GWR analysis confirmed the local impact of NDBI, MNDWI, and NDVI on the dynamics of the LST of each city. Since the analysis of GWR shows the largest R^2 and the smallest AIC in the four cities, the goodness of fit of the GWR model was boosted to 0.51, 0.47, 0.66, and 0.63 for Addis Ababa, Adama, Hawassa, and Bahir Dar cities, respectively, from the goodness of fit test fit of the OLS 0.49, 0.40, 0.64, and 0.61 in the earlier order. This means that the GWR was explained by 52% of the LST dynamics on average. While the OLS model explains

Table 8
Comparison of the fitting effect between the GWR model and OLS model (2020).

Model	Fitting factors	Bahir Dar	Adama	Addis Ababa	Hawassa
GWR	R-Squared	0.63	0.47	0.51	0.66
	R^2 Adjusted	0.63	0.44	0.50	0.64
	Akaike info criterion	22342.98	21291.91	22205.14	22755.16
	Schwarz orientation	22024.40	21012.50	22129.20	22294.5
	−2 log-likelihood:	22332.98	20954.21	22126.96	22497.57
OLS	R-Squared	0.61	0.40	0.49	0.64
	R^2 Adjusted	0.60	0.40	0.48	0.63
	Akaike info criterion	22998.30	21986.50	22203.10	22768.50
	Schwarz orientation	23024.40	22012.50	22229.20	22794.50
	−2 log-likelihood:	−11495.10	−10989.10	−11097.20	−11380.20

48% of LST changes on average. This indicated that the GWR model could better explain LST change at the local level, as the fitting effect for the GWR model was 4% higher than that for the OLS model. Thus, compared with the OLS model, it is reasonable and feasible to use the GWR for analysis of remote sensing indexes and the LST change nexus.

4. Discussion

4.1. Effects of landscape changes on urban heat island intensities (UHIs)

Results showed that all the selected four major cities expanded unceasingly from 1990 to 2020. Although, the economic development and population density rate varied substantially among them. For example, Addis Ababa is the only metropolitan in Ethiopia and about a quarter of the urban population in Ethiopia lives in it [8,10,60]. [59] scrutinized the spatial patterns of major cities in Ethiopia and found a similar conclusion, that is, urbanization in the major cities of Ethiopia was very rapid. Furthermore, urban agglomerations were meaningfully interrelated with the population growth and rural to urban migration, economic growth, and structural transformation of the major cities of Ethiopia [8,15]. According to Ref. [8]; the built-up landscape of major cities of Ethiopia was augmented by 17,341.0 ha (32.2%), 2151.3 ha (19.6%), 2715.2 ha (12.2%), and 2599.7 ha (15.7%) for Addis Ababa, Adama, Bahir Dar, and Hawassa, respectively over the past three periods (Figs. 3–4). Besides, the sensitivity of LST to urbanization-induced landscape change is one of the interesting phenomena in the research era [5,14,35]. Our results also confirmed that the presence of relationships between LST and urbanization-induced influencing factors (Table 6). For instance, in all cities the observed sensitivity of LST to urban forest and greenery, water body change is negative [31,61,63,67], but the degree of offsetting of UHI intensity was varied with time change across the cities. On the other hand, the manifested sensitivity of LST to urbanization-induced influencing factors is positive and amplified with the time change across the cities. The principal source of the inconsistency of sensitivity of LST, cities is not a simple aggregation of the independent system while it is of a combination of many complex systems and the hub of the manifold interactions, like biogeochemical cycle and urban metabolic processes [9,11,22]. Thus, the output was revealed sensitivities that are substantially varied from natural landscape sensitivities. In this study, for example, Hawassa and Bahir Dar have large water bodies, while relatively low industrialization and anthropogenic actively as compared to Addis Ababa and Adama do not have large water bodies. Conversely, analysis of the spatial relation between the LST and non-remote sensing variables may provide a tangible indicator for the need for urban landscape resilience [3,8,10,61].

Furthermore, high-temperature zones in the cities augmented analogies with this urbanization pattern. The overall expansion of temperature zones also was followed the cities agglomeration from an initially urbanized center to multi-direction outskirt spatial patterns. For example, in 2020, the spatial distribution of High-temperature zones of Addis Ababa, Hawassa, Adama, and Bahir Dar was increased by 3109ha (50%),723ha (23%), 989ha (86%), and 2456ha (66%) from 1990 respectively and resulting in the rapid evolution of the spatial pattern of UHIs (Fig. 5). On the other hand, the coverage and cooling intensity of urban forests and the greenery of the thermal environment declined with the time change. In the present study, 30% of Addis Ababa, 16% of Bahir Dar, 11.38% of Adama, and 5.55% of Hawassa urban forest and greenery were converted to built-up landscapes in the past three decades. This scenario was also reported by other scholars [36,40,49,61,64]. In addition, unsustainable urbanization would lead to changes in the overall urban landscape types [8,71], the disturbed balance of earth surface radiation and energy [38], influenced ecosystem services demand and supply [1], as well composition of near-surface atmospheric water budget [28,43] and ultimately affected the spatial pattern of urban as well as the regional thermal environment [21,22]. In this study, the increasing rate of urbanization significantly influenced the temporal and spatial evolutions of LST.

4.2. The influences of remote sensing indexes on LST evolution

The single variable Pearson correlation coefficient of LST with the selected seven explanatory variables shows substantial variations of correlations in cities with the time changes (Table 5). NBDI, MNWDI, and NDVI are consistently affect LST ($P < 0.05$) [7,18,20,57,61]. [20] showed a positive strong correlation of LST with NDBI, while NDVI indicates a negative relationship ($P < 0.05$) in Addis Ababa. These finding also shows that built up landscapes in Addis Ababa substantially contributed for evolution UHI effect, whereas urban forest and greenery could regulate the intensity of UHI effect [52]. also reported the existence of a strong correlation of NDBI (0.89) with LST and could increase the UHI effect in cities. Thus, rapid urban agglomeration and urban landscapes change (high NDBI) is might be upsurged sensible heat change on the ground [11,54], and anthropogenic heat emission [1,17,68] and the electric consumption of the cities also influenced by LST and NDBI nexus [33] and the strength of UHI evolution [54,55].

In this study, the offsetting effect of urban forest and greenery (i.e., NDVI-LST correlation) was varied with time, for example, in Addis Ababa (64% in 2010), followed by Adama (63% in 2000), Hawassa (59% in 1990), and Bahir Dar (48% in 2010), and the weakest effect was observed in Adama (19% in 2020). In addition, trends of urbanization rate with the time show stronger UHI effect on an artificial surface, the relatively the weakest the mitigating contribution from the existed urban forestry and greenery, because the NDBI-NDVI nexus significantly (negative) influenced and reduced the heat-trapping potential of water vaouper which released form plants via evapotranspiration. For example [56], reported the cooling intensity of vegetation in cities of chines varied with a range of 40%–60% to correlate with UHI effects of landscape dynamics. Similarly [16], reported that the substantial development of the impervious area and UHI intensity in the peri-urban parts of Delhi was highly correlated (negatively) with the vegetation landscapes change [14]. also reported the rapid urbanization of Lagos was significantly declined the size of the green area by converted to build up and resulting in increased UHI through the time change. In general, this phenomenon is found due to the complexity of the urban landscape and urbanization interaction [41,73]. Thus, LST–NDBI, and LST–NDVI had stronger correlations in large built-up areas and

natural landscapes respectively.

Further, this study specified that water bodies (MNDWI) could mitigate UHI intensity by 50% on average (Table 5). A moderately significant negative correlation was found in Hawassa and Bahir Dar, even if it varied with time changes. The main reason associated with this is the presence of Lake Hawassa and Lake Tana, which play a vital role in the decrease of LST through evapotranspiration in Hawassa and Bahir Dar, respectively. However, the relative humidity of both cities is slightly higher than in Addis Ababa, which might lead to an increase in moisture content in the atmosphere and warm up the air because water vapor is an efficient atmospheric greenhouse gas (Li et al., 2017; Sheng et al., 2017; [56]. While Addis Abeba and Adama had the lowest (negative) correlation between MNDWI and LST (Table 5), it could have a significant impact on the quality and quantity of water bodies, as well as positively contribute to changing the thermal environment [61]. On the other hand, the correlation of LST with other influencing factors is not always significant, and the effect also varies among cities. For example, the relationship between LST and geographical location (latitude and longitude) shows a moderate correlation in Bahir Dar and Hawassa, both positively and negatively. While population density and altitude variation do not contribute significantly to UHI evolution in almost all cities (Table 5), Wang et al. (2021c) discovered that anthropogenic factors contribute slightly more to UHI than natural drivers in 16 major Chinese cities.

4.3. Spatial dependence on LST-remote sensing nexus

The interface between spatial dependence on LST varies with urbanization time, according to multivariate regression analysis on influencing factors on LST in this study. Overall, the coefficient of OLS (spatial lag model and spatial error model) analysis might change with time; nonetheless, the sign is constant (i.e., positive or negative effect on LST with time). In contrast, remote sensing indexes (NDBI, MNDWI, and NDVI) became the most dominant influencing factors and significantly determined the spatial distribution of UHI for each city at certain periods (Tables 5 and 6). In addition, the error coefficients (LAMBDA) in SEM for Addis Ababa, Adama, Bahir Dar, and Hawassa cities were significantly positive at $p < 0.01$ in the past three decades, which means that the LST of the cities was positively influenced by neighboring values. Although the regression coefficients of MNDWI and NDVI were negative. This demonstrates the strong positive relationships that exist between LST and NDBI. This means that increasing urbanization has had a significant impact on the evolution of urban heat island intensities as well as the declining offset of urban forest and greenery and water bodies [8,9,56,61,72].

In this study, we also analyzed geographic location and elevation factors as governing features for LST changes in each city. However, the finding is not significant in most cities (Takkanon & Chantarangul 2019), urbanization and urban agglomeration rate. Furthermore, studies show that climate influences on UHI intensities are correlated with variations in moisture (Tran et al., 2006; Li et al., 2021) and water body size. In the present study, the rift valley cities (i.e., Adama and Hawassa) found higher air moisture content compared with the highland city (i.e., Addis Ababa) and showed relatively larger urban-rural differences in air moisture, resulting in higher LST differences between urban and surrounding areas. While Addis Ababa is large in size and urbanization rate, the climate effects are also related to urban canyon effects (Takkanon & Chantarangul 2019) and the evolution of UHI differences are higher in the outskirts of the city. In addition, geographical location is indirectly affected by UHI intensities by regulating vegetation conditions and surface albedo (Takkanon & Chantarangul 2019; Alexander 2021).

In this study, we also analyzed the association between LST and seven factors by using the GWR and OLS models for all cities. The OLS model is commonly used to compute the association between LST and influencing factors [61]; Zhu et al., 2020). However, the precision of the model will be reduced when we introduce no significant explanatory independent variables into the model [56]. Thus, we used SLM and SEM models to optimize the fit of the regression equation. The LST was positively spatially correlated with the remote sensing index NDBI and negatively correlated with MNDWI and NDVI as shown by bivariate Global Moran's I. Additionally, on account of spatial autocorrelations, SRMs (SLM and SEM) were found to be more appropriate than OLS regression for assessing the spatial dependence of LST on NDBI, MNDWI, and NDVI. The lag coefficient (W_ESV) in SLM for Addis Ababa in 1990 was negatively significant ($p < 0.01$). The error coefficients (LAMBDA) were significantly negative at $p < 0.01$ in SMEs for Adama, Hawassa, Bahir Dar, and Addis Ababa in the past three decades. The spatial regression results showed that LST dependence on the remote sensing indexes is changing slightly. Besides, in this study, we recognized a spillover (hidden) influence on the LST and remote sensing index nexus. Thus, the LST of cities is also affected by other factors in addition to remote sensing indexes. On the other hand, the results and diagnostics of the GWR model show that it has better predictive power than OLS and SRMs for all selected cities. In addition, the Akaike's Information Criterion (AIC) value, Schwarz orientation, and −2 log-likelihood, which are used to compare the efficiency of models, substantially declined (Table 7). Overall, the GWR model generated more reliable results compared to the OLS model across all cities. This finding indicates that local-based models provide more rationale and a realistic relationship between LST and its remote sensing indexes. Such a finding was also supported also in earlier studies [8]; Kashki et al., 2021). Besides, GWR is used to detect higher temperature zone where UHI mitigating strategies may need to focus on these factors.

4.4. Implications for green city resilience and future research

Our study can potentially support green city resilience in several aspects. First, the manifested sensitivities of LST to influencing factors should guide the selection of possible offsetting mechanisms that prevent urban LST from going up spirally. Second, this study has offered novel empirical evidence and applied pieces of analysis that enable comparison among cities to identify UHI changes in the most rapidly accelerating cities. Third, using compared OLS and SRMs, this study investigates the effect of multiple factors on HUL magnitude and spatial dependence. As a result, if the findings of this study are used elsewhere, they will fill some gaps in current scientific studies. Despite these implications, this research has some limitations: Firstly, the remaining spillover influencing factors

need also to be studied deeply (i.e., urban size and traffic flow). Second, we used medium-resolution imagery for LULC classes, but high-resolution imagery should be used for a more detailed classification of LULC and a better understanding of the drivers' factors-UHI nexus.

5. Conclusions

Urbanization and climate change phenomena point to a dire need to know which factors alter land surface temperature, thus, we might establish mitigation measures to sustain environmental comfort and ultimately improve the quality of life in cities. The present study describes the dynamics of urban green space and LST over 30 years (from 1990 to 2020) in the major cities of Ethiopia. Our goal was to assess how these dynamic nexuses, along with MNDWI, NDVI, NDBI, and major urbanization factors, influenced LST intensity and UGS cooling intensity deterioration. The study area, during the period specified, underwent increases in the mean values of the NDBI and UHI intensity, while also showing reductions in the mean values of NDVI and MNDWI. The urban ecosystem dynamics reflect substantial increases in built-up coverage, accompanied by decreases in water bodies, urban green space, forest, and urban agriculture coverage. Besides, the spatial distribution of UHI intensity is wide-ranging among cities and In 1990, the high-temperature zone was the epicenter of urban core areas. In contrast, by 2020, high-temperature regions on the outskirts of each city would have been aggravated. The dominant governing factors in each city change over time and affect LST intensity significantly. According to the spatial regression model equation of LST, the coefficient values of the principal governing factors were changed. Additionally, on account of spatial autocorrelation, SRMs were found to be more appropriate than OLS regression for assessing the spatial dependence of LST on remote sensing indexes. Thus, the findings can have practical (political) implications for cities' urban green space and forest management. The mapping, identification, and geostatistical analysis of UGS and LST vulnerable to urban heat effects can be useful for improving the assessment of the cities' UGS states (the quality of their ecosystem services), indicating where adapting greening practices and planting tree species can promote urban green space and forest resilience to the effects of LST.

Author contribution statement

Mekonnen Amberber Degefu, PhD; Mekuria Argaw, PhD; Gudina Legese Feyisa, PhD; Sileshi Degefa, PhD: Conceived and designed the experiments; Performed the experiments; Analyzed and interpreted the data; Contributed reagents, materials, analysis tools or data; Wrote the paper.

Funding statement

This research did not receive any specific grant from funding agencies in the public, commercial, or not-for-profit sectors.

Data availability statement

Data included in article/supp. material/referenced in article.

Declaration of interest's statement

The authors declare no competing interests.

References

[1] M. Amberber, M. Argaw, G.L. Feyisa, S. Degefa, Status, approaches, and challenges of ecosystem services exploration in Ethiopia: a systematic review, Chin. J. Pop. Res. Environ. 18 (2020) 201–213.
[2] Y. Cai, Y. Chen, C. Tong, Spatiotemporal evolution of urban green space and its impact on the urban thermal environment based on remote sensing data: a case study of Fuzhou City, China, Urban For. Urban Green. 41 (2019) 333–343.
[3] J. Chen, S. Jin, P. Du, Roles of horizontal and vertical tree canopy structure in mitigating daytime and nighttime urban heat island effects, Int. J. Appl. Earth Obs. Geoinf. 89 (2020).
[4] W. Chen, G. Chi, J. Li, The spatial association of ecosystem services with land use and land cover change at the county level in China, 1995–2015, Sci. Total Environ. 669 (2019) 459–470.
[5] L.W. Chew, X. Liu, X.-X. Li, L.K. Norford, Interaction between heat wave and urban heat island: a case study in a tropical coastal city, Singapore, Atmos. Res. 247 (2021), 105134.
[6] CSA, Central Statistical Agency of Ethiopia, ICPS- Population Projection 2007- 2037 Produced in 2012, 2020. https://www.statsethiopia.gov.et/wp-content/uploads/2019/05/ICPS-Population-Projection-2007-2037-produced-in-2012.pdf.
[7] N. Das, P. Mondal, S. Sutradhar, R. Ghosh, Assessment of variation of land use/land cover and its impact on land surface temperature of Asansol subdivision, Egypt. J. Rem. Sen. Space Sci. 24 (2021) 131–149.
[8] M.A. Degefu, M. Argaw, G.L. Feyisa, S. Degefa, Dynamics of urban landscape nexus spatial dependence of ecosystem services in rapid agglomerate cities of Ethiopia, Sci. Total Environ. 798 (2021), 149192.
[9] M.A. Degefu, M. Argaw, G.L. Feyisa, S. Degefa, Effects of urbanization on the relationship between greenspace patterns and evolution of regional heat island in cities of Ethiopia, Chin. J. Pop. Res. Environ. 19 (2021) 330–343.
[10] M.A. Degefu, M. Argaw, G.L. Feyisa, S. Degefa, Impact of landscape dynamics and intensities on the ecological land of major cities in Ethiopia, Environ. Sys. Res. 10 (2021) 32.
[11] M.A. Degefu, M. Argaw, G.L. Feyisa, S. Degefa, Regional and urban heat island studies in megacities: a systematic analysis of research methodology, Indoor Built Environ. 31 (2022) 1775–1786.

[12] K. Degirmenci, K.C. Desouza, W. Fieuw, R.T. Watson, T. Yigitcanlar, Understanding policy and technology responses in mitigating urban heat islands: a literature review and directions for future research, Sustain. Cities Soc. 70 (2021), 102873.
[13] K. Deilami, M. Kamruzzaman, Modelling the urban heat island effect of smart growth policy scenarios in Brisbane, Land Use Pol. 64 (2017) 38–55.
[14] D. Dissanayake, T. Morimoto, Y. Murayama, M. Ranagalage, H.H.J.S. Handayani, Impact of urban surface characteristics and socio-economic variables on the spatial variation of land surface temperature in Lagos City, Nigeria 11 (2019) 25.
[15] P. Dorosh, J. Thurlow, Can cities or towns drive african development? Economywide analysis for Ethiopia and Uganda, World Dev. 63 (2014) 113–123.
[16] D. Dutta, A. Rahman, S.K. Paul, A. Kundu, Impervious surface growth and its inter-relationship with vegetation cover and land surface temperature in peri-urban areas of Delhi, Urban Clim. 37 (2021), 100799.
[17] I. Dutta, A. Das, Exploring the Spatio-temporal pattern of regional heat island (RHI) in an urban agglomeration of secondary cities in Eastern India, Urban Clim. 34 (2020).
[18] A.-A. Faisal, A.-A. Kafy, A. Al Rakib, K.S. Akter, D.M.A. Jahir, M.S. Sikdar, et al., Assessing and predicting land use/land cover, land surface temperature and urban thermal field variance index using Landsat imagery for Dhaka Metropolitan area, Environ. Challeng. 4 (2021), 100192.
[19] J. Feranec, G. Hazeu, B. Kosztra, S. Arnold, in: J. Feranec, T. Soukup, G. Hazeu, G. Jaffrain (Eds.), CORINE Land Cover Nomenclature. *European Landscape Dynamics: CORINE Land Cover Data*, 2016, pp. 17–25.
[20] G.L. Feyisa, H. Meilby, G. Darrel Jenerette, S. Pauliet, Locally optimized separability enhancement indices for urban land cover mapping: exploring thermal environmental consequences of rapid urbanization in Addis Ababa, Ethiopia, Rem. Sens. Environ. 175 (2016) 14–31.
[21] K. Fuladlu, Thermal Response to Land-Use Land-Cover Patterns: an Experimental Study in Famagusta, Cyprus, CLEAN – Soil, *Air, Water*, n/a, 2022, 2100284.
[22] K. Fuladlu, M. Riza, M. Ilkan, THE EFFECT OF RAPID URBANIZATION ON THE PHYSICAL MODIFICATION OF URBAN AREA, 2018.
[23] D.H. García, Analysis of urban heat island and heat waves using sentinel-3 images: a study of andalusian cities in Spain, Earth Sys. Environ. 6 (2022) 199–219.
[24] S. Guha, H. Govil, A. Dey, N. Gill, Analytical study of land surface temperature with NDVI and NDBI using Landsat 8 OLI and TIRS data in Florence and Naples city, Italy 51 (2018) 667–678.
[25] G. Guo, Z. Wu, Z. Cao, Y. Chen, Z. Yang, A multilevel statistical technique to identify the dominant landscape metrics of greenspace for determining land surface temperature, Sustain. Cities Soc. 61 (2020), 102263.
[26] B. Halder, A. Karimi, P. Mohammad, J. Bandyopadhyay, R.D. Brown, Z.M. Yaseen, Investigating the relationship between land alteration and the urban heat island of Seville city using multi-temporal Landsat data, Theor. Appl. Climatol. (2022) 1–23.
[27] Y. Hu, L. Zhen, D. Zhuang, Assessment of land-use and land-cover change in Guangxi, China, Sci. Rep. 9 (2019) 1–13.
[28] F. Huang, W. Zhan, Z.-H. Wang, J. Voogt, L. Hu, J. Quan, et al., Satellite identification of atmospheric-surface-subsurface urban heat islands under clear sky, Rem. Sens. Environ. 250 (2020), 112039.
[29] Y. Jiang, W. Lin, A Comparative Analysis of Retrieval Algorithms of Land Surface Temperature from Landsat-8 Data, vol. 18, A Case Study of Shanghai, China, 2021, p. 5659.
[30] J.C. Johnson, J. Urcuyo, C. Moen, D.R.J.P.o. Stevens, Urban Heat Island Conditions Experienced By The Western Black Widow Spider (Latrodectus Hesperus): Extreme Heat Slows Development But Results In Behavioral Accommodations, 2019, e0220153, 14.
[31] A.-A. Kafy, A. Al Rakib, K.S. Akter, Z.A. Rahaman, A.-A. Faisal, S. Mallik, et al., Monitoring the effects of vegetation cover losses on land surface temperature dynamics using geospatial approach in Rajshahi City, Bangladesh, Environ. Challeng. 4 (2021), 100187.
[32] A. Kaiser, T. Merckx, H.J.E. Van Dyck, Evolution, The Urban Heat Island And Its Spatial Scale Dependent Impact On Survival And Development In Butterflies Of Different Thermal Sensitivity, 2016, pp. 4129–4140, 6.
[33] S. Kamboj, S. Ali, Urban sprawl of Kota city: a case study of urban heat island linked with electric consumption, Mater. Today Proc. 46 (2021) 5304–5314.
[34] S.W. Kim, R.D. Brown, Urban heat island (UHI) intensity and magnitude estimations: a systematic literature review, Sci. Total Environ. 779 (2021), 146389.
[35] R. Kotharkar, A. Ramesh, A. Bagade, Urban heat island studies in south asia: a critical review, Urban Clim. 24 (2018) 1011–1026.
[36] W. Leal Filho, F. Wolf, R. Castro-Díaz, C. Li, V.N. Ojeh, N. Gutiérrez, et al., Addressing the Urban Heat Islands Effect: A Cross-Country Assessment of the Role of Green Infrastructure, vol. 13, 2021, p. 753.
[37] H. Li, Y. Zhou, X. Li, L. Meng, X. Wang, S. Wu, et al., A new method to quantify surface urban heat island intensity, Sci. Total Environ. 624 (2018) 262–272.
[38] L. Li, Y. Zha, J. Zhang, Spatially non-stationary effect of underlying driving factors on surface urban heat islands in global major cities, Int. J. Appl. Earth Obs. Geoinf. 90 (2020), 102131.
[39] X. Li, W. Li, A. Middel, S. Harlan, A. Brazel, B. Turner, Remote sensing of the surface urban heat island and land architecture in Phoenix, Arizona: combined effects of land composition and configuration and cadastral–demographic–economic factors, Rem. Sens. Environ. 174 (2016) 233–243.
[40] X. Li, W. Zhou, Z. Ouyang, W. Xu, H. Zheng, Spatial pattern of greenspace affects land surface temperature: evidence from the heavily urbanized Beijing metropolitan area, China, Landsc. Ecol. 27 (2012) 887–898.
[41] H. Liu, Q. Zhan, C. Yang, J. Wang, The multi-timescale temporal patterns and dynamics of land surface temperature using Ensemble Empirical Mode Decomposition, Sci. Total Environ. 652 (2019) 243–255.
[42] L. Liu, X. Chen, W. Chen, X. Ye, Identifying the impact of landscape pattern on ecosystem services in the middle reaches of the yangtze river urban agglomerations, China, Int. J. Environ. Res. Publ. Health 17 (2020) 5063.
[43] T. Lu, X. Cui, Q. Zou, H. Li, Atmospheric water budget associated with a local heavy precipitation event near the Central Urban Area of Beijing Metropolitan Region, Atmos. Res. 260 (2021), 105600.
[44] H.L. Macintyre, C. Heaviside, X. Cai, R. Phalkey, The winter urban heat island: impacts on cold-related mortality in a highly urbanized European region for present and future climate, Environ. Int. 154 (2021), 106530.
[45] Q. Mao, J. Peng, Y. Wang, Resolution enhancement of remotely sensed land surface temperature: current status and perspectives, Rem. Sens. 13 (2021) 1306.
[46] M.A. McGeehin, M.J.E.h.p. Mirabelli, The Potential Impacts Of Climate Variability And Change On Temperature-Related Morbidity And Mortality In The United States, 2001, pp. 185–189, 109.
[47] National Meteorology Agency, National Meteorological Station Report. Federal Democratic Republic of Ethiopia, Addis Ababa, 2020. http://www.ethiometmaprooms.gov.et/.
[48] C. O'Malley, P. Piroozfar, E.R.P. Farr, F. Pomponi, Urban Heat Island (UHI) mitigating strategies: a case-based comparative analysis, Sustain. Cities Soc. 19 (2015) 222–235.
[49] J. Peng, J. Ma, Q. Liu, Y. Liu, Y. Hu, Y. Li, et al., Spatial-temporal change of land surface temperature across 285 cities in China: an urban-rural contrast perspective, Sci. Total Environ. 635 (2018) 487–497.
[50] M. Rahman, A. Ahmad, X. Wang, A.f.t.a.b. Wajid, W.a.j.i.d. Nasim, M. Hussain, et al., Multi-model projections of future climate and climate change impacts uncertainty assessment for cotton production in Pakistan, Agric. For. Meteorol. (2018) 253–254.
[51] I. Rousta, M. Sarif, R. Gupta, H. Olafsson, M. Ranagalage, Y. Murayama, et al., Spatiotemporal analysis of land use/land cover and its effects on surface urban heat island using landsat data: a case study of metropolitan city Tehran (1988–2018), Sustainability (2018) 10.
[52] A. Sekertekin, E. Zadbagher, Simulation of future land surface temperature distribution and evaluating surface urban heat island based on impervious surface area, Ecol. Indicat. 122 (2021), 107230.
[53] I. Senanayake, W. Welivitiya, P. Nadeeka, Remote sensing based analysis of urban heat islands with vegetation cover in Colombo city, Sri Lanka using Landsat-7 ETM+ data, Urban Clim. 5 (2013) 19–35.
[54] P. Shahmohamadi, A. Che-Ani, K. Maulud, N. Tawil, N.J.U.S.R. Abdullah, The Impact of Anthropogenic Heat on Formation of Urban Heat Island and Energy Consumption Balance, 2011, 2011.
[55] R. Sharma, L. Pradhan, M. Kumari, P. Bhattacharya, Assessing urban heat islands and thermal comfort in Noida City using geospatial technology, Urban Clim. 35 (2021), 100751.
[56] Y. Shi, S. Liu, W. Yan, S. Zhao, Y. Ning, X. Peng, et al., Influence of landscape features on urban land surface temperature: scale and neighborhood effects, Sci. Total Environ. 771 (2021), 145381.

[57] S.A. Shiflett, L.L. Liang, S.M. Crum, G.L. Feyisa, J. Wang, G.D. Jenerette, Variation in the urban vegetation, surface temperature, air temperature nexus, Sci. Total Environ. 579 (2017) 495–505.
[58] S. Siddique, M.M. Uddin, Green space dynamics in response to rapid urbanization: patterns, transformations and topographic influence in Chattogram city, Bangladesh, Land Use Pol. 114 (2022), 105974.
[59] B.K. Terfa, N. Chen, D. Liu, X. Zhang, D. Niyogi, Urban expansion in Ethiopia from 1987 to 2017: characteristics, spatial patterns, and driving forces, Sustainability 11 (2019).
[60] J. Vandercasteelen, S.T. Beyene, B. Minten, J. Swinnen, Big cities, small towns, and poor farmers: evidence from Ethiopia, World Dev. 106 (2018) 393–406.
[61] Y. Wang, G. Yi, X. Zhou, T. Zhang, X. Bie, J. Li, et al., Spatial distribution and influencing factors on urban land surface temperature of twelve megacities in China from 2000 to 2017, Ecol. Indicat. 125 (2021), 107533.
[62] Z. Wang, Q. Meng, M. Allam, D. Hu, L. Zhang, M. Menenti, Environmental and anthropogenic drivers of surface urban heat island intensity: a case-study in the Yangtze River Delta, China, Ecol. Indicat. 128 (2021), 107845.
[63] G. Worku, E. Teferi, A. Bantider, Assessing the effects of vegetation change on urban land surface temperature using remote sensing data: the case of Addis Ababa city, Ethiopia, Remote Sens. Appl.: Soci. Environ. 22 (2021), 100520.
[64] J. Yang, J. Sun, Q. Ge, X. Li, Assessing the Impacts of Urbanization-Associated Green Space on Urban Land Surface Temperature: A Case Study of Dalian, China, vol. 22, Urban Forestry & Urban Greening, 2017, pp. 1–10.
[65] G.T. Yengoh, D. Dent, L. Olsson, A.E. Tengberg, C.J. Tucker III, Use Of The Normalized Difference Vegetation Index (NDVI) To Assess Land Degradation At Multiple Scales: Current Status, Future Trends, And Practical Considerations, Springer, 2015.
[66] Z. Yu, Y. Yao, G. Yang, X. Wang, H. Vejre, Strong contribution of rapid urbanization and urban agglomeration development to regional thermal environment dynamics and evolution, For. Ecol. Manag. 446 (2019) 214–225.
[67] J. Zelený, D. Mercado-Bettín, F. Müller, Towards the evaluation of regional ecosystem integrity using NDVI, brightness temperature and surface heterogeneity, Sci. Total Environ. 796 (2021), 148994.
[68] H. Zhang, L.G. Zhou, M.N. Chen, W.C. Ma, Land use dynamics of the fast-growing Shanghai Metropolis, China (1979-2008) and its implications for land use and urban planning policy, Sensors 11 (2011) 1794–1809.
[69] L. Zhang, W. Liu, K. Hou, J. Lin, C. Song, C. Zhou, et al., Air pollution exposure associates with increased risk of neonatal jaundice, Nat. Commun. 10 (2019) 3741.
[70] Y. Zhang, Y. Liu, Y. Zhang, Y. Liu, G. Zhang, Y. Chen, On the spatial relationship between ecosystem services and urbanization: a case study in Wuhan, China, Sci. Total Environ. 637–638 (2018) 780–790.
[71] Y. Zhang, T. Zhang, Y. Zeng, C. Yu, S. Zheng, The rising and heterogeneous demand for urban green space by Chinese urban residents: evidence from Beijing, J. Clean. Prod. 313 (2021), 127781.
[72] Z.-Q. Zhao, B.-J. He, L.-G. Li, H.-B. Wang, A. Darko, Profile and concentric zonal analysis of relationships between land use/land cover and land surface temperature: case study of Shenyang, China, Energy Build. 155 (2017) 282–295.
[73] Z. Zhao, A. Sharifi, X. Dong, L. Shen, B.-J. He, Spatial variability and temporal heterogeneity of surface urban heat island patterns and the suitability of local climate zones for land surface temperature characterization, Rem. Sens. 13 (2021) 4338.